

# Texture for Colors: Natural Representations of Colors Using Variable Bit-Depth Textures

Shumeet Baluja  
Google, Inc.  
San Diego, USA



**Figure 1:** Transformation of color images to textured, single-bit, images. Similar colors are represented by similar textures, thereby allowing smooth gradients in the original to be visually smooth in the binary image as well. The chosen textures accurately model the intensity variations and edges of the original image. Additionally, the textures are fully reversible; based solely on the binary texturized image, the full color original image can be recreated. From left to right: *The Church at Auvers* (1890) by Vincent van Gogh, *The Warrior Miura-no-suke Confronting the Court Lady Tamamo-no-ma* (1820) by Yashima Gakutei, black and white photograph of a young girl reading (2020), and a portion of *Color Study. Squares with Concentric Circles* (1913) Wassily Kandinsky.

## ABSTRACT

Numerous methods have been proposed to transform color and grayscale images to their single bit-per-pixel binary counterparts. Commonly, the goal is to enhance specific attributes of the original image to make it more amenable for analysis. However, when the resulting binarized image is intended for human viewing, aesthetics must also be considered. Binarization techniques, such as half-toning, stippling, and hatching, have been widely used for modeling the original image’s intensity profile. We present an automated method to transform an image to a set of binary textures that represent not only the intensities, but also the colors of the original. The foundation of our method is information preservation: creating a set of textures that allows for the reconstruction of the original image’s colors solely from the binarized representation. We present techniques to ensure that the textures created are not visually distracting, preserve the intensity profile of the images, and are natural in that they map sets of colors that are perceptually similar to patterns that are similar. The approach uses deep-neural networks and is entirely self-supervised; no examples of good vs. bad binarizations are required. The system yields aesthetically pleasing binary images when tested on a variety of image sources.

## KEYWORDS

Non-photorealistic rendering, machine learning, stippling, e-ink, subtractive manufacturing, low bit-rate images

## 1 INTRODUCTION

For more than half of a century, numerous methods have been proposed to transform images to their binarized counterparts — where each pixel is represented by a single on/off bit [20]. At the highest level, these approaches can be categorized into two sets: those intended for human viewing and those intended as a pre-processing step for one specific task. When created for human-viewing, the images created are typically more aesthetically pleasing and maintain a broader set of the original image’s attributes at the expense of losing specific details useful for specialized analysis. Common techniques include stippling, hatching and edge-based approaches. Early examples of cross hatching in Western art, where hatches and cross hatches were used to represent a scene’s most salient image colors and features can be traced back to the Middle Ages [71]. In modern usage, for example in newspapers, a variety of stippling approaches are employed. These are described in the next section.

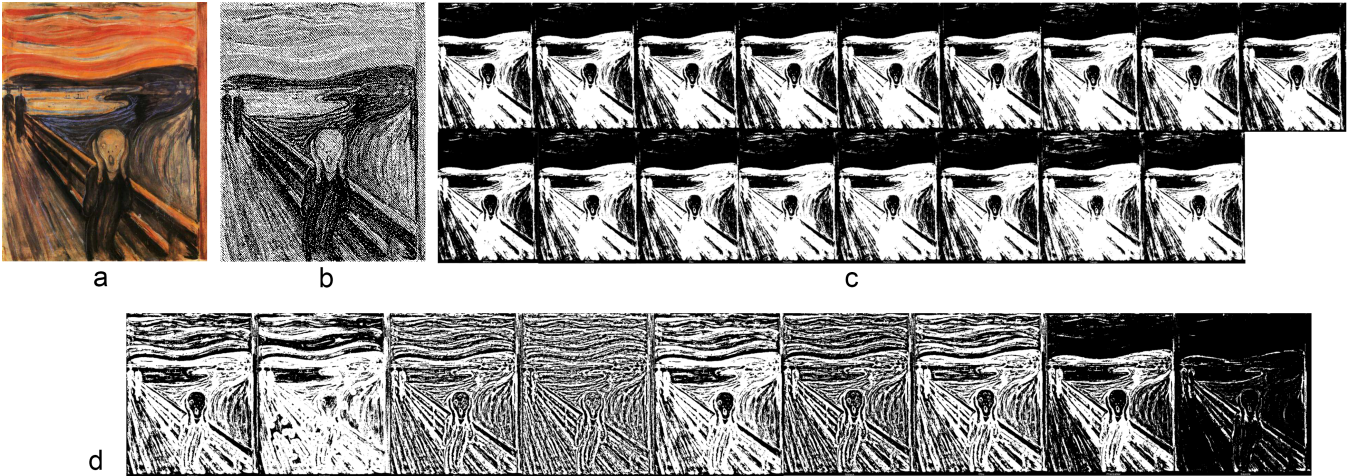


**Figure 2:** 26 approaches for creating a binary image. (a) *The Scream* by Edvard Munch (1893). (b) Our approach. (c) 17 global-thresholding methods (shown small, no detail is preserved). (d) 9 local-techniques.

Beyond artistic interest, binarization is commonly used in a variety of scenarios. Popular electronic-book readers [26], such as Kindle [3], Boox [48], and Nook [5], as well as public digital signage [70, 16] all use e-ink with varying levels of bit-depth. Binary texture images are the basis for a large set of subtractive fabrication processes. These include water-jet, laser-cutting with thin materials (paper, cloth, *etc.*) [24], or popular home cutting devices [12].

We introduce a method to create selectable-bit-rate images from color or grayscale originals by automatically synthesizing a texture representation of the image. We concentrate on the hardest case of a binary image with a single bit per pixel. Nonetheless, the techniques are trivially modified to address representations with any number of bits. Even with just a single bit, the full color image can be reconstructed from the result. Additionally, images that contain colors that are similar in intensity/luminance, or any dimension that is commonly used for setting thresholding points or for converting color to grayscale, will also be represented with distinguishable textures. In contrast to recent deep-steganographic techniques [30, 4], there are no low-order bits to effectively hide the original’s color information. Instead, all the information must be encoded into the *visible* features – the textures that are created; see Figure 1.

Two fundamental challenges must be addressed to create an effective system. In the standard 3-channel 8-bit RGB representation, there are  $2^{24}$  different colors possible. Beyond the difficulties associated with the number of unique textures required to represent each possibility, we cannot utilize a unique texture for every pixel, as each is given only 1-bit in the binarized image. Instead, our method selects which colors to represent based on the prevalence of colors in the images we wish to model (*e.g.* natural images). It also learns to adaptively combine spatially close pixels in the original image to create a texture representative of localized regions.

Second, we must assign the textures to the colors judiciously – such that the resulting binary image does not introduce extraneous edges. For this, it is important that colors that are visually similar have visually similar textures. We refer to this as a *natural* ordering

of the textures; the textures seamlessly blend into each other when smooth transitions of colors are present in the original image.

This paper makes five contributions. First, we have created a system that transforms any full color image into a reduced bit-depth gray or pure black and white representation. The approach does not require iterative search or relaxation techniques; a single forward pass through a deep neural network is used. Second, we demonstrate how our method achieves natural textures such that visually similar colors are represented with similar textures. Third, within the learning framework of deep neural networks, we present both novel architectures and novel error functions to help capture aesthetic preferences. Fourth, we demonstrate how we can recover the original colors from the binary textures. Fifth, we briefly note how we alleviate some of the biases in machine learning systems related to skin color by working towards more accurate accounting for complexion differences and color representation.

## 2 RELATED WORK

There is a wealth of literature on approaches to binarize/threshold images; many survey articles provide a comprehensive history [61, 54, 9, 10, 57, 64]. In Figure 2c, examples of 17 *global* thresholding methods are shown. Global thresholding approaches compute statistics from the entire image to decide where to place a single threshold to create the binary cutoff. Shown are two versions of Huang fuzzy thresholding [31], Prewitt’s method with bimodal histograms [52], IsoData [55], Minimum Cross Entropy [41], MaxEntropy [23], Min-Error [37], Prewitt’s method with histogram smoothing [52], Moment preservation [67], Otsu [49], foreground/background splitting assuming 50% of each [15], Renyi Entropy [35], Shanbhag [62], Triangle Method [74], and Yen’s method for multilevel thresholding [73]. Methods were computed using the *ImageJ* toolkit [54, 59, 2]. As noted by Lee et al. [40], global thresholding works well when the pixel intensities in the image form a bimodal histogram and the object of interest is large in comparison to the image size. However, issues arise when the object of interest is small compared to the size of the image, when there is low contrast between the foreground



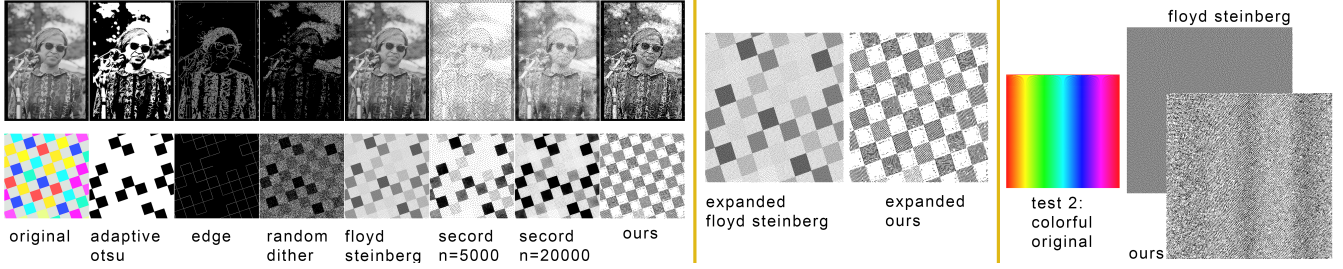


**Figure 3:** Image binarization intended for human viewing. (left) Original Image, Otsu Adaptive, edge detection [7], random dithering, Floyd-Steinberg (FSD) Dithering [43], Secord Voronoi with point sizes from 1 to 20 (5000 points), Secord Voronoi with 20,000 [56], and our method. (middle) Zoomed images of tilted square image binarized with FSD and our method. FSD cannot distinguish similar intensity squares, despite different colors. Our method can capture them since we operate on full color images. (right) All colors are lost with FSD and methods that use only a single channel. In contrast, our approach considers all channels.

and background pixels, when the image, or object of interest, has non-uniform illumination or the image is degraded with significant noise. As can be seen in Figure 2c, the majority of the details have been removed in all of the binarized results.

In Figure 2d, results from nine *local* thresholding techniques are presented. These methods compute a cutoff threshold based on the intensity statistics of surrounding pixels. The results include the Bernsen method [6], local toggle contrast [63], mean, median and mid-gray thresholding based on local statistics [17], Niblack [47], localized Otsu [49], Phansalkar [50], and Sauvola [58]. The local approaches outperform the global by maintaining more details and shading and intensity variations.

In contrast to the task-specific approaches above, the next set of techniques are more often used for creating binarizations suitable for human viewing, for example in newspapers. Common techniques in this class of approaches include stippling methods [19] such as dithering, half-toning and stroke-based approaches that include hatching and edge detection, see Figure 3. Here, the distribution of dots is vital to the perception of the underlying image. The canonical method is based on error diffusion [18]. Intensity can also be modeled with variable size dots. Secord’s approach based on Voronoi regions has yielded compelling results [60, 56]; samples are shown in Figure 3. Hatching and cross-hatching use variable length and thickness lines oriented in parallel, crossing, or contoured orientations. Prominent automated approaches have tackled shading and contours for complex objects [75, 51, 34]. Edge-detection also falls into this category of line-based representations of images.

We have observed Floyd-Steinberg dithering and methods such as the Linde-Buzo-Gray preserve details from the original [14]. However, there is an underlying limitation to these approaches: they must operate on grayscale images when the desired goal is a single bit-per-pixel (1-bpp) image. If the original has colors, the first step is to convert it into a single channel [28]. All standard conversion operations lose information that will yield disparate colors indistinguishable. In contrast, with our system, all three channels are considered; the image is *not* first converted to grayscale, allowing us to encode and recover the colors solely from the binary image (Figure 3-right).

The closest work to ours in terms of motivation is *Color2Gray* [25]. *Color2Gray* attempted to handle the isoluminant variations that

were not preserved with standard color to grayscale conversions through explicitly analyzing chrominance and luminance differences. Like [25], we handle isoluminance; however, we employ an information-preservation perspective and dramatically reduce bit rates. Similar problems have arisen in numerous specialized applications [53] that require converting photographs to stylized bi-tonal renderings. In terms of the approach taken, the closest work is [72]. They use a CNN to convert color to grayscale and back; the work parallels the deep-steganography mentioned earlier. Their architecture is a subcomponent of the one presented here. For example, to achieve 1bpp while maintaining smooth transitions in colors, their method requires augmentation with both the novel loss functions and the architectural mechanisms that will be presented.

A note about the relationship of this work to style transfer [22, 21], GANs [45, 27], and Image-to-Image Translation [32, 42, 76]. Our initial approaches to synthesizing a binary image from a full color image was to use GANs within the unsupervised image-to-image translation process and numerous style-transfer approaches. Though good results were sometimes obtained, there were severe drawbacks. With style-transfer, the same color on different original images were not consistently mapped to the same textures – an intuitive expectation. Second, in order to ensure that the result was 1-bpp, the majority of the contributions presented here, the architectures and loss functions, were needed to supplement all the approaches. Finally, the GAN training process was significantly less stable than using explicit information-preservation as the basis of our objective function. The final system described here did not require an adversarial teacher. This yielded a simpler and more stable to train system. It also provided consistency in color mappings across images, and generated at least equal, and most often superior, results.

### 3 LEARNING TEXTURES

In our work, we attempt to represent unconstrained complex scenes (full photographs, paintings, artwork) as binary images. In designing our approach, the seven most salient desiderata are:

- (1) *Different perceived colors should have different texture representations.* The representation chosen for a color should not solely depend on any single dimension (e.g. intensity).

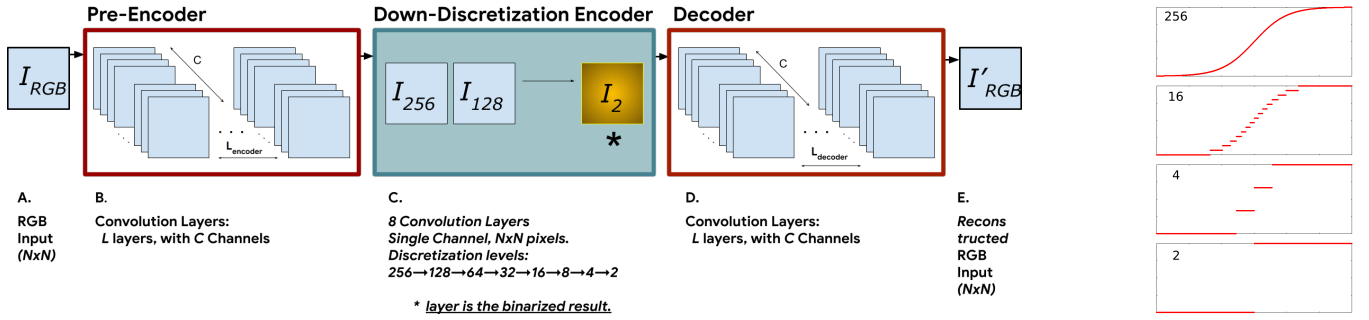


**Figure 4:** (left) A fully convolutional network architecture to transform an  $n \times n$  24-bpp RGB image into an  $n \times n$  1-bpp binary image. We cast the problem as a reformulation of an auto-encoder network with explicit constraints on the bottleneck’s representation. Note that the entire decoder module is used exclusively in training; we need it to compute the error that is used to train the system:  $L_2(I_{RGB} - I'_{RGB})$ . The actual image that will be shown to the user, the binarized image, is marked with an asterisk (\*). (right) The discretized  $\tanh$  activation functions for 4 of the 8 layers in the *Down-Discretization Encoder* (256,16,4,2)

- (2) Colors that are visually similar are represented by similar textures.
- (3) The same color in different images should be represented similarly. This allows the reconstruction of the original’s colors and matches intuitive expectations.
- (4) The textures introduced to represent colors should not be visually distracting. The prominent edges in the original should be the only ones visible under normal viewing magnification.
- (5) The approach should be extendable to variable bit-rates. Some e-ink displays have a 2-level display, while other widely deployed e-readers, such as Kindle, have 16 [3].
- (6) In addition to representing the colors of the original image, images without color (e.g. grayscale originals) should also work.
- (7) We should not have to manually create textured images to train the system.

Given the desiderata described above, let us first consider the simplest solution: mapping every color to a unique texture and simply using a lookup table. To implement this approach, first, we would need to decide which discretization of colors to consider, since, as mentioned earlier,  $2^{24}$  textures is unwieldy. Second, after a discretization scheme is chosen, how should we measure similarity for this task? Should hue, intensity and saturation be weighted equally, or should alternate perceptual metrics be used? Third, we cannot replace a single pixel with a full texture, therefore we must decide on how to create regions to model together. Will this involve static blocks or adaptive region growing? Fourth, how are transitions from one color to the next handled in the binarized image? If this is handled poorly, edges will appear in the image. Colors that often occur together must have compatible textures to avoid creating visual discontinuities in the binarized image as a result of minor color transitions in the original image.

Instead of attempting to manually find a mapping from colors to textures, we use a learning approach. It is grounded in the following observation: if the colors are represented uniquely in the transformed image, then we should be able to invert this process, e.g. reconstruct the full color image from just the binary image. The remaining desiderata are achieved through the specifics of

the training procedure as well as the novel loss functions that are employed.

To begin, let us examine the well established principles of auto-encoder neural networks [38, 33, 39, 65]. An auto-encoder network is a self-supervised architecture to learn a compressed representation of the input data. The *encoder* portion of the auto-encoder learns to transform an input image to a substantially reduced dimensionality (similarities to principal components analysis are explored in [38]). This is accomplished by passing the input (an image) through a series of non-linear transformations, including a low-dimensional “bottleneck” layer. The *decoder* portion of the auto-encoder manipulates the internal compressed representation emitted by the bottleneck to recreate the original image.

Through the backpropagation of errors between the original input and its reconstruction after the decoding, the encoder learns to compress information about the original image through the bottleneck. For images of resolution  $n \times n$ , a bottleneck of size  $m$  is used where  $m \ll n \times n$ . Simultaneously, the decoder learns to use that representation to reconstruct the image. Recently, reductions in transmission size competitive with state-of-the-art image and video compression have been obtained through auto-encoder based approaches [66, 46].

We use the same principle, but instead of reducing the number of dimensions, we reduce the representational capacity of each dimension. For generating binary images, our equivalent to the bottleneck layer keeps the same image dimensions as the original,  $n \times n$ ; however, each dimension can only represent two values:  $\{0,1\}$ . A network architecture to implement this is shown in Figure 4.

Note that the reduction of colors to binary is accomplished within the *Down-Discretization Encoder* module (see Figure 4, Box C). Here, the bits per pixel in the image are successively lowered to 1-bit per pixel (bpp). The input that the *Down-Discretization Encoder* module receives is an internal representation based on the original 24bpp image. The output of the module is the desired 1-bpp image.

Figure 5 provides a visual explanation of the transformations in the *Down-Discretization Encoder*. The original image, in the leftmost column, is a full 24-bpp image. It is transformed by the Pre-Encoder to an internal representation of  $128 \times n \times n$  floating point numbers. This is used as the input to the *Down-Discretization Encoder*. The



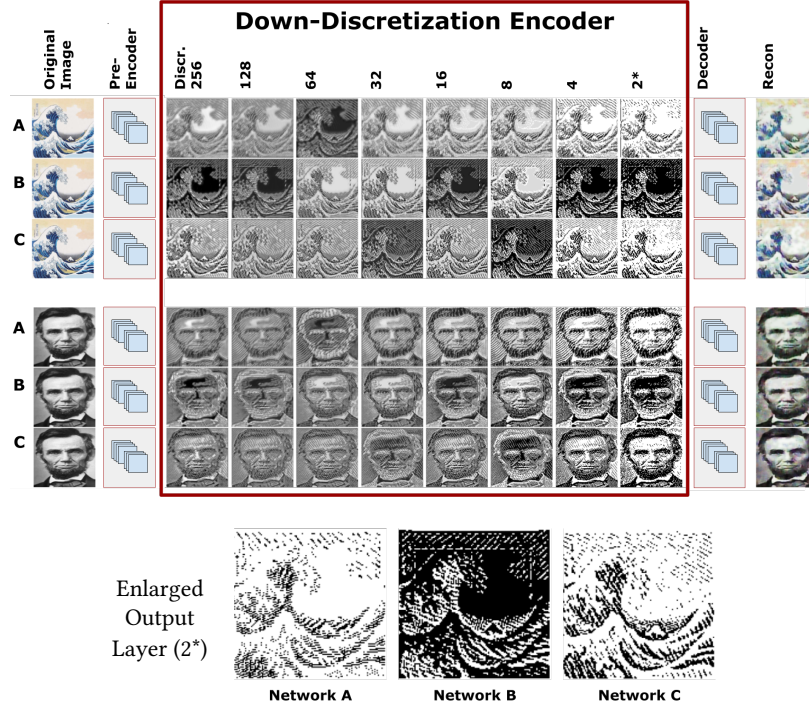


**Figure 5:** (Top) The eight down-discretization steps shown for two images, *The Great Wave off Kanagawa* (1829-1833) by Hokusai and a portrait of Abraham Lincoln. The original image is leftmost (24 bit, RGB). This is passed through the pre-encoder. The next column, “Discretized-256”, shows the output of the first Down-Discretization layer, in which each pixel can be 1 of 256 values (8bpp). The next 7 layers reduce the image to binary by each removing 1 bit. The actual output that the user is given is the last one in the *Down-Discretization Encoder* (marked with (\*)). All layers after the *Down-Discretization Encoder* are only used for training. The operations of three independently trained networks (A-C) are shown. (Bottom) Enlarged versions of the binary images generated. Note the variations resulting solely from the stochasticity in training between all three networks, including the inversion of intensities in Network B.

first discretization layer receives this input and produces a single channel  $n \times n$  8-bpp image. This is fed into the next discretization layer through a single (trained) convolution kernel and a single channel 7-bpp image is produced. This process is repeated until there a 1-bpp image. Note that each layer’s discretized-tanh activation introduces a non-linear transformation, as shown in Figure 4. The final layer’s output from the *Down-Discretization Encoder* is the binary image that is shown to the end-user (marked with “\*”).

When training the system, the binary image emitted by the *Down-Discretization Encoder* is propagated through the decoder module. The decoder reconstructs the colors of the original image from the binarized representation. The network is trained to minimize the error between the reconstruction and the original. When successfully trained, the textures in the binarized image uniquely identify the underlying colors that generated the pattern.

Why should textures arise? The key insight is that textures *must* arise in order to successfully reduce the reconstruction error. Consider the alternative: an architecture in which the reconstruction of each pixel was based on a single pixel of  $\{0,1\}$  values. The color information required for reconstruction could not be encoded. By using convolution layers that allow nearby pixels to be considered, groups of nearby pixels convey a region’s color information. However, since we have constrained the system so that *the only*

*information transmitted is through the visible binary image*, the information encoding of nearby pixels takes the form of *visible* patterns; these patterns are precisely the textures desired.

For our first trial, we used the network shown in Table 1. We begin our experimentation by simply minimizing the reconstruction error:  $L_2(I_{RGB} - I'_{RGB})$ . ImageNet photographs (without labels) are used for training [13]; the inputs and outputs were  $128 \times 128$  pixels. The networks were trained with Tensorflow, using Adam optimization [1, 36] with  $LR = 0.0001$ , batch size=16 and uniform noise added to the inputs of  $\pm 5\%$ . To handle training in the presence of the discretizations employed in the *Down-Discretization Encoder*, we discretized the values from the units in all of the forward passes (training and inference). However, in the backward error propagation step of training, the discretizations were ignored and the underlying function (tanh) was used instead; this is a straight-through-estimator [29].

Results of the initial tests were shown in Figure 5 and are expanded upon in Figure 6. The binarized image produced by network A and C (Figure 5) appear reasonable, but network B produces a color-inverted image. This inversion occurs because there is no information loss by inversion and therefore reconstruction error (our sole measurement so far) is not affected. Note that both networks A and C suffer from this in earlier stages of the down-discretization

**Table 1:** Network architecture. Each layer uses  $(3 \times 3)$  convolutions. (The final binarized output is marked with \*)

	input	layers, channels per layer	activation function	activation function in last layer	output
Pre Encoder	24 bit $n \times n$	10, 128	relu	relu	128 float $n \times n$
Down Discretization Encoder	128 float $n \times n$	8, 1	tanh discrete <sub>256</sub> - discrete <sub>4</sub>	tanh discrete <sub>2</sub>	<b>1 bit</b> $n \times n$ (*)
Decoder	1 bit $n \times n$	10, 128	relu	tanh	24 bit $n \times n$

procedure. This is not just a problem of inversions; rather, it occurs because there are no constraints for matching the original’s intensities in the *Down-Discretization Encoder*. We will address this next, in Section 3.1.1.

In the expanded results in Figure 6, note that the images’ colors are successfully represented by different textures. The reconstructions, which are solely based on the patterns in the binary image, recreate the colors well, though are noisy – indicating that some color information is not recovered. Recall, however, that the reconstruction is *not* the end product in this task; it is never shown to users. Its only purpose is to compute the training loss. An unwanted large discontinuity in the binary textures is shown in Figure 6d. This flaw occurs because visually similar colors in the original are *not* constrained to similar texture representations. This can cause the perception of edges where they do not exist in the original. In Section 3.1.2, we will describe how to improve this.

Though the intent of our procedure is to create textures for binarized images, we note that the textures created are reversible. They can be converted back into colors (as shown in the triplets in Figure 6a-c). This occurs because the reconstruction error is minimized in the training process. We will return to this in Section 5.

### 3.1 Algorithmic Improvements

Numerous extensions and improvements were attempted. Those that had the largest impact are described here.

**3.1.1 Relative Intensity Constraints.** To avoid the mistake shown in Figure 5, in which dark regions in the original may be represented with bright textures, intensity constraints are introduced.

We need to ensure that the relative brightness of region<sub>*j*</sub> vs. region<sub>*k*</sub> in the original image,  $I$ , matches the relative brightness of region<sub>*j*</sub> vs. region<sub>*k*</sub> in the binary image  $I_2$ . We divide  $I$  into  $r$  non-overlapping equally sized regions, and compute each’s average intensity. The result is reshaped into a column vector,  $A$ , of length  $r^2$ . Next, we compute the difference in intensities for each pair of regions,  $A' = A \cdot 1^T - 1 \cdot A^T$  (the  $1$  column vector is of length  $r^2$ ). The differences are scaled to  $[-1.0, 1.0]$ .

The corresponding matrix,  $B''$ , is computed for  $I_2$ . With this, we compute the magnitude of the relative differences,  $|A'' - B''|$ . The lower this value, the more the differences in region intensities *within* the original images match the region differences *within* the binarized image. This measurement (Equation 1) is used to supplemental the  $L_2$ -reconstruction loss described earlier. In our tests, we set  $r = 8$ .

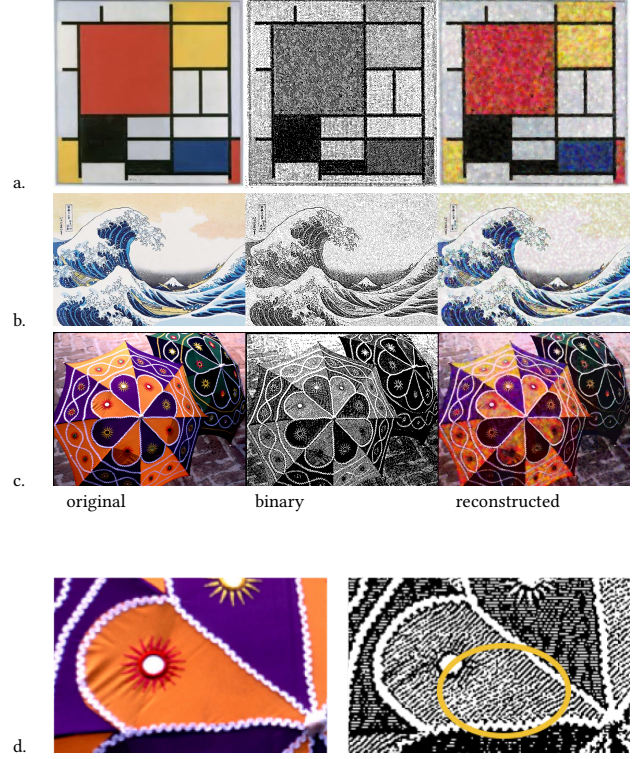


**Figure 6:** Samples from initial trial. In each triplet (a,b,c), the original (left), binary(middle), and reconstruction solely from the binary (right) are shown. (a) Mondrian (1921): different colors are represented with different textures. (b) Colorful umbrella photograph. (c) The wave’s shape is clearly visible, but the white appears gray. (d) A mistake from the umbrella photograph is shown enlarged: a drastic shift in textures does not correspond to a large change in the original’s colors.

$$L_{relative\_intensity} = |tanh(A \cdot 1^T - 1 \cdot A^T) - tanh(B \cdot 1^T - 1 \cdot B^T)| \quad (1)$$

We note that this step is particularly important to address the sensitive topic of hidden biases in the training and evaluation of machine learning methods. Without this step, varying skin-tones were mapped to textures that appeared similar. There was little distinction between paler and darker complexions. Adding this step significantly improved the distinctions in the resulting binary images between light and dark skin tones.

**3.1.2 Color Continuity Constraints.** To avoid the mistake shown in Figure 6, we need to ensure that similar colors are represented by compatible textures. Let us consider a family of modification operators,  $M(I)$ , that perturb the input  $I$ , such that the colors in  $I$  are shifted by a small amount. If the modification operators we consider yield images that appears similar in terms of color, then by ensuring that the textures used for the colors in  $I$  match the textures for  $M(I)$ , we ensure that similar colors are represented similarly, see Equation 2. The network transforms the input  $I$  into



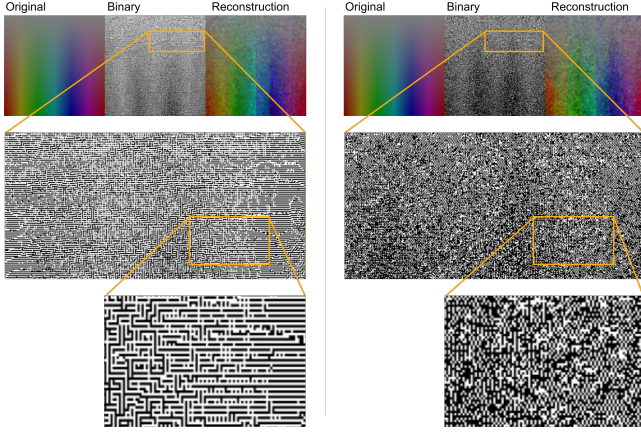


**Figure 7:** Discretization of the same image using two separately trained network to examine color continuity. When smooth regions of the image are examined, we hope to find correspondingly smooth changes in the binarized image. (left): Within the zoomed image, notice that the pattern of texture changes rapidly. (right): The change of patterns is far more subtle; this network was trained with color continuity constraints.

the binary image  $I_2$ , this is noted as  $encode_2(I)$ .

$$L_{color\_continuity} = |encode_2(I) - encode_2(M(I))| \quad (2)$$

In training, in each batch, even numbered images are replaced with a modification of the previous odd-numbered image. The simplest modification operator is used: independent noise per pixel. This effectively keep two copies of the image, with and without perturbation, in the batch — the goal is ensure that they both have similar binary encodings. For example, Figure 7C shows a poor transformation where nearby colors are represented with large texture shifts. In (E), the same region is shown for a network trained with color continuity loss.

**3.1.3 Handling Uncommon Colors.** In training the initial system, real photographs from ImageNet were used. However, when the system was tested, often the first test users performed was on paintings, clip art, or other artwork. To better address the distribution of colors present in these image classes, we augmented the training set with synthetically generated images.

The synthetic images were rendered with a background of constant color. Two to five shapes (ovals and rectangles) were added to the image, in random colors, sizes, and aspect-ratios, without considering overlap. All color selections were made uniformly randomly from the set of  $2^{24}$  possible choices. These generated examples were used to replace  $S\%$  of each batch in training. Numerous settings of  $1\% \leq S \leq 50\%$  were tested. Empirically,  $S = 10\%$  worked well; it had a noticeable impact on how well artwork and clip art were binarized while photograph performance was unchanged.

## 3.2 Neural Architectures

Finding the appropriate neural network for this task required numerous architecture decisions and extensive empirical testing. For our study, the decisions can be broadly categorized into three

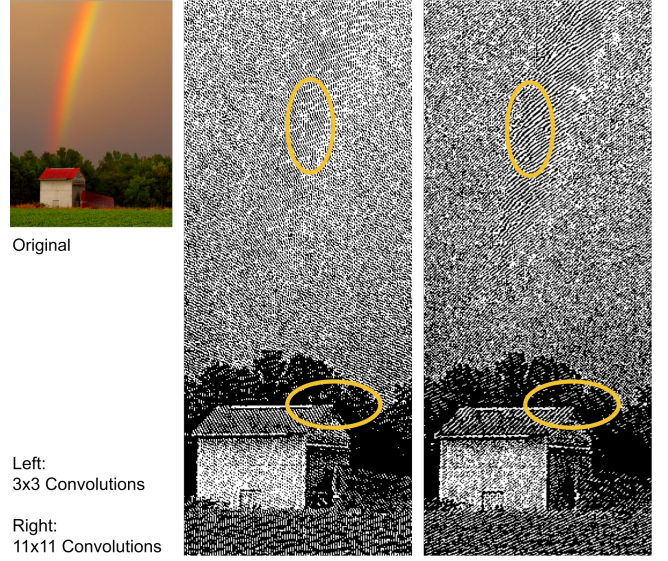


**Figure 8:** Effects of convolution size on diversity of textures produced in the binary image. In the expanded views, notice how the  $11 \times 11$  convolution network is able to yield varied textures for the rainbow, tree-lines and roof.

branches: convolution sizes, discretization progression, and network connectivity, specifically the number and size of hidden layers.

Within the image-understanding community, the use of convolutions in neural networks is standard practice. The size of the convolution is vital since it controls the integration of information across the image [11, 69, 44]. Though image classification systems commonly use  $3 \times 3$  convolutions, these did not yield the best results here. Larger convolutions are able to create a larger variety of textures, see Figure 8.

Experiments were conducted with convolutions of size  $2 \times 2$ – $11 \times 11$ . Consistently, larger convolution sizes provided more appealing results than smaller ones. However, the perceptible differences between larger sizes diminish. Because increasing the size of the convolutions rapidly increases the training times, for our final system, all the convolutions were  $6 \times 6$ .

When discretizing layers in neural networks, often the reduction from full floating point to a lower bit-depth representation occurs in a single step. In contrast, as shown in Figure 5, the *Down-Discretization Encoder* gradually steps down the discretization from 8-bpp to 1-bpp. We also tested the more common single-step approach, as well as eliminating only selected intermediate depths. Though all of the methods provided acceptable results, the gradual step-down procedure consistently yielded better results.

Though beyond the scope of this paper, the largest set of experiments conducted are those that tuned the network architecture and learning parameters. Finding “the right” number of layers and connectivity patterns is largely a trial-and-error endeavor. For example, we experimented with using (2-20 layers), as well as a wide variety of number of channels (10-150) per layer. The majority of early exploration also employed equal size pre-encoder and decoders, as is common practice. An unexpected finding was that a large decoder

was not only unnecessary, but could be detrimental. In the final system, the decoder and pre-encoder were asymmetric. The decoder was reduced to only 2 layers, while the pre-encoder remained 10 layers. We postulate that a smaller decoder is beneficial because it forces the binary image to appear as close as possible to the final image by not permitting large transformations of the binary image to create the reconstruction. Full details on the selected network architecture are provided next.

### 3.3 Learning Summary

In designing the final system, numerous, diverse architectures, loss functions, and network training meta-parameters (gradient descent algorithm, non-linear activation functions, learning rate, *etc.*) were explored. In total, 980 different networks were trained. The single network chosen is specified in Table 2. The final loss to be minimized was ( $\alpha = 0.1$  and  $\beta = 0.1$ ):

$$\begin{aligned} Total\_Error = & L_2(I_{RGB} - I'_{RGB}) \\ & + (\alpha \times L_{relative\_intensity}) \\ & + (\beta \times L_{color\_continuity}) \end{aligned} \quad (3)$$

For our training set, 90% of the examples were photographs from ImageNet. The remaining 10% were synthetically generated. The same Tensorflow parameters for training described earlier were used again. The training time on a single Nvidia-P100 GPU was approximately 36 hours.

For the final network selection, we whittled the trials from the GANs, style transfer networks, and the 980 architectural variants to 25. This pruning was based on a cursory scan of the resulting images and the magnitude of the reconstruction errors. With these 25 sets of remaining images, an independent user-interface expert was asked to examine the images generated by all 25 networks and select those that created the binary image that best represented the original. Neither the reconstructed image nor any of the other network feature were considered or even revealed. The network that obtained the most votes is shown in Table 2. A total of 150 images were evaluated in this phase. During the evaluation process, the majority of the initial 25 networks received no votes, suggesting that a few networks clearly outperformed the rest<sup>1</sup>.

## 4 EXPERIMENTS AND RESULTS

Figure 9 shows the results of using the selected final network (Table 2) on 18 images drawn from a variety of sources. (a) shows the results on artwork that contains colors outside the range of standard photographs. In the photographs in column (b), note that the changes in hue as well as intensity are successfully captured in the

<sup>1</sup>Having conducted this extensive network exploration, we must re-emphasize that training neural networks is a fundamentally stochastic procedure. The performance of the same network can vary based on the order the training samples are presented, the training times, the initial randomly selected network weights, and the meta-parameters, to name a few. This fact, coupled with the qualitative nature and inherent noise in ascertaining which binarized image appears better than another, makes it difficult to definitively assert that the single architecture selected is better than all the rest. Due to stochasticity in training, a different set of parameters or random initial weights might have changed the performance. If replicating the system, we suggest training several networks, even with the architecture and parameters found here, to overcome outliers in performance.

**Table 2:** Final architecture. Each layer uses  $(6 \times 6)$  convolutions. Note the asymmetric pre-encoder and decoder sizes. The final binarized output is marked with \*. (Difference from previous architecture is highlighted.)

	input	layers, channels per layer	activation function	activation function in last layer	output
Pre Encoder	24 bit $n \times n$	10, 128	relu	relu	128 float $n \times n$
Down Discretization Encoder	128 float $n \times n$	8, 1	tanh discrete <sub>256</sub> - discrete <sub>4</sub>	tanh discrete <sub>2</sub>	<b>1 bit</b> $n \times n$ (*)
Decoder	1 bit $n \times n$	<b>2, 128</b>	relu	tanh	24 bit $n \times n$

binary representation. With the darker images in (c), the intensity changes are vital to capture. Note that the “pop-out” brightness of the moon on the night-sky is captured (photographs 1 & 3 in column c). The black and white originals in (d) demonstrate that although the network was not trained on any grayscale images, the binarization is successful.

In Figure 9e, expanded views show details of the textures synthesized for four results (the bottom image of each column). In (e), notice the variety of textures and clear boundaries between distinct regions. In (f), similar textures are employed to represent all the wood pieces in the bench; these give the sense of similarity between the pieces and the continuity of each slat. In (g), the different fireworks are easily distinguishable through the use of textures. In (h), the same (or similar) textures are automatically chosen for the beard, resulting in natural appearing shading. Additional results are shown in Figure 1 and the Appendix.

In Figure 10(top), we provide four examples to elucidate the limitations of our approach. In (a), the low contrast in the image obscures the water/sky boundary in the binarized image. In (b), though the regions are identifiable, without color, the image is difficult to interpret. In (c) the tiger is difficult to see due to similarities in the orange and brown textures. In (d) we see the most insidious of cases for our system: pointillism. In Seurat’s *A Sunday on La Grande Jatte* (1884), the painting is created with tiny dots of various hues and saturations. The rapid changes in color as well as the many discontinuities are difficult. Reducing the size of the image (and thereby averaging the pixels) or simply blurring the image before generating the binary representation will improve results.

Finally, we present four images specifically created to test our system, Figure 10(bottom). These provided controlled tests to measure the diversity of colors being represented and how color transitions are handled. Figure 10e is a gradient background image with text written in various intensities (the number is the intensity value out of 255) (f) repeats this test with a pure black and white background. Figure 10(g&h) examine smooth and abrupt color changes.

## 5 CONCLUSIONS AND FUTURE WORK

We presented an automated method to replace a color or grayscale image with a set of binary textures that not only represent the original image’s colors and patterns well, but adhere to the aesthetic and pragmatic desiderata stated in Section 2:



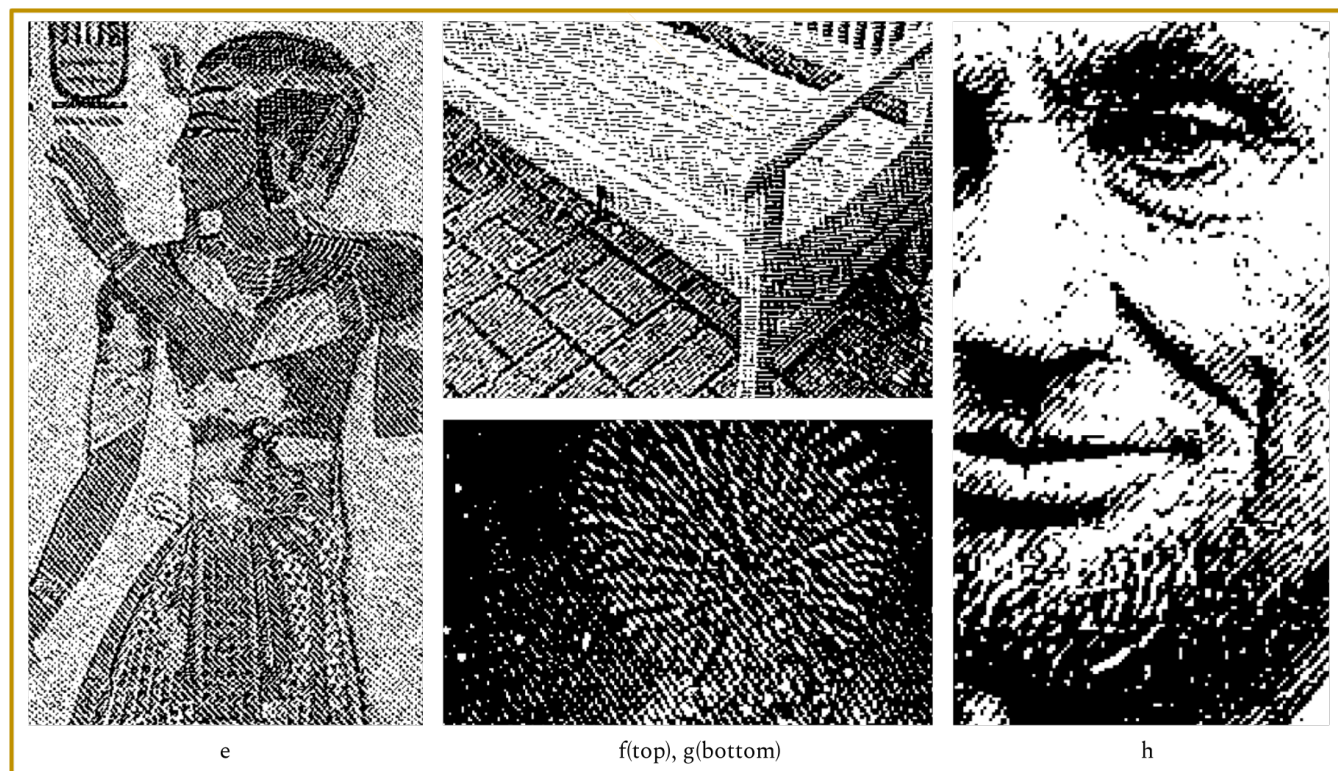
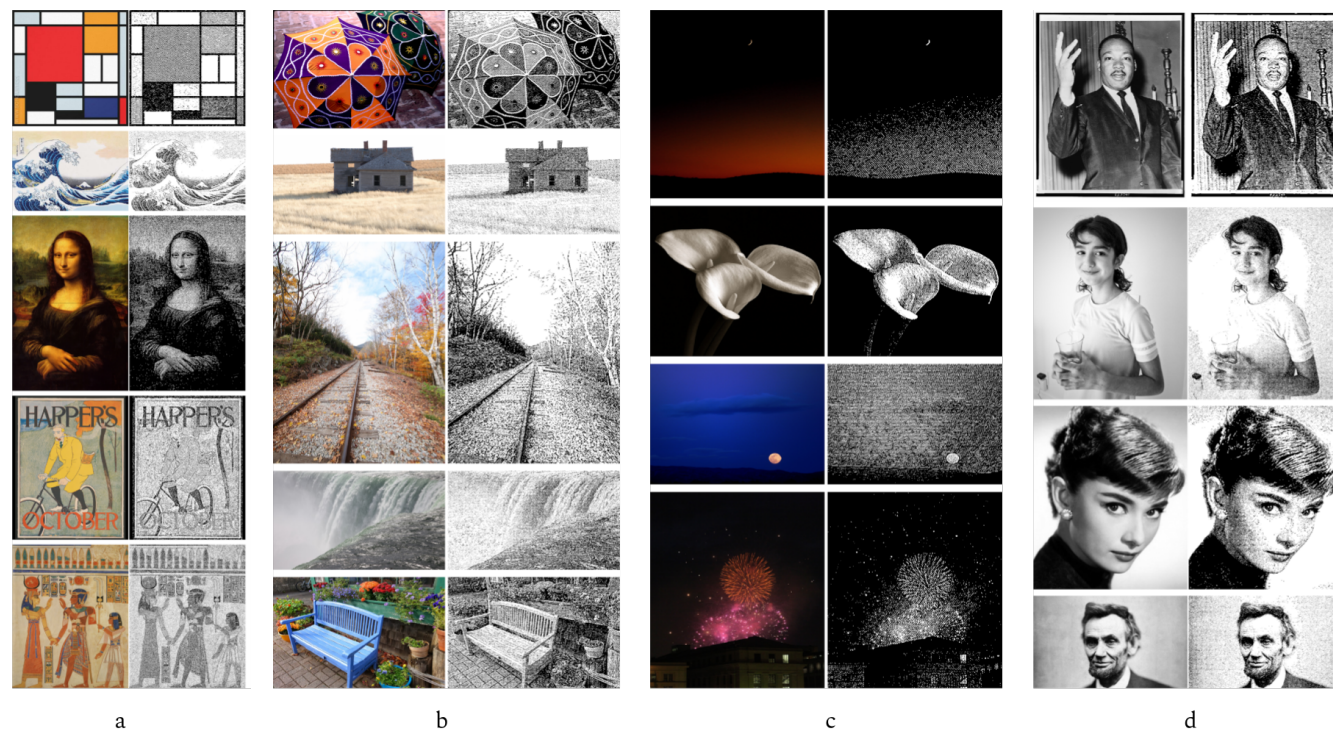


**Figure 9:** Results in four categories: (a) paintings and art, (b) photographs, (c) dark images, and (d) black and white source images. Enlarged views of the bottom-most images in each category shown within the orange rectangle (e-h). Please see text for full description.



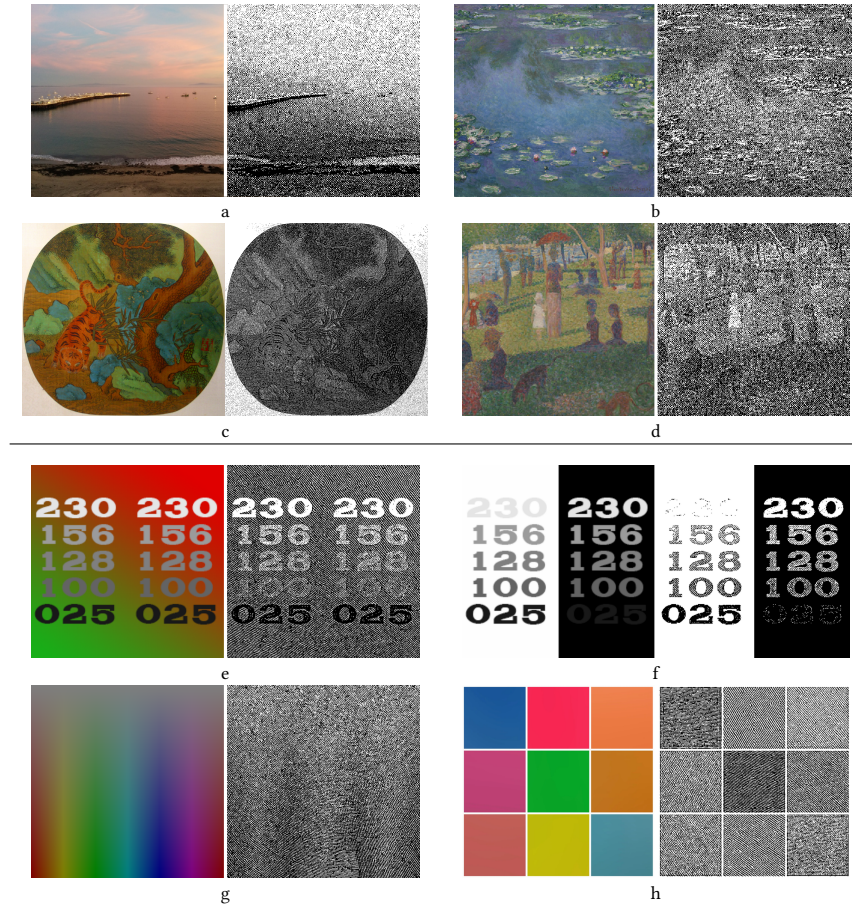


**Figure 10:** Limitations of our approach. a,b: A lack of contrast yields too little sky/water distinction in the photograph and in Monet’s *Water Lilies* (1914). c: *Tiger Drinking from a Stream* (Qing Dynasty period) the tiger appears camouflaged due to the similar texture representation of these shades of orange and brown. d: Seurat’s pointillism; the colors in close proximity to each other result in no coherent patterns. Bottom section: four explicit tests to examine smoothness and color representation range. e,f: Various backgrounds with foreground numbers in the gray-level indicated by the number. g,h: Smooth and abrupt color boundaries.

- (1) *Different perceived colors have different texture representations.* This is satisfied through the training procedure; the system is trained to ensure that we can recreate the original color image from the binary representation.
- (2) *Colors that are visually similar are represented by similar textures.* This was explicitly addressed with the continuity loss described in Section 3.1.2.
- (3) *Different images have the same color represented similarly.* This can be seen by the ability to reconstruct the original’s colors using the same “decoder” module.
- (4) *The textures introduced to represent colors are not visually distracting.* See Figure 9 and the Appendix.
- (5) *The approach should be extendable to variable bit-rates.* The extension to other bpp rates is built into the system and is trivial to instantiate. For example, to reduce the final representation to 4-bpp instead of 1-bpp, we need only remove the last 3 layers in the *Down-Discretization Encoder* and retrain.

- (6) *The proposed method should work equally well for grayscale images as for color images.* As shown in Figure 9, grayscale images are treated the same as color images; no extra steps were taken to handle these.
- (7) *No manual specification of good vs. bad binarizations.* The system is entirely **self-supervised**. There were no manually created examples of good and bad binarizations. Instead, the system was trained through the principle of information preservation.

Though an integral portion of our system, the reconstruction error was solely employed during training. In usage, we discard the decoder and no longer compute the reconstruction error. Nonetheless, in some applications, the reconstruction may be a valuable product as well, e.g. for low-bandwidth transmission of an image that can be converted back into color. In this regard, we note that there are explicit knobs for controlling the quality of the reconstruction vs. the quality of the binarization. The most effective is the size of the decoder (which was reduced in the final architecture



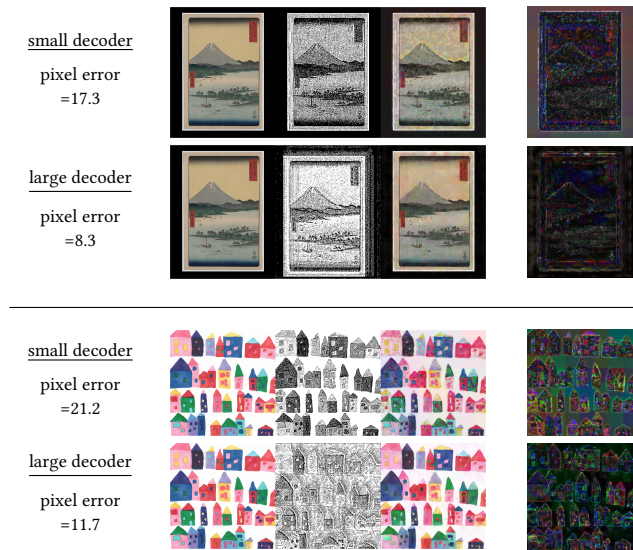


**Figure 11:** Notice the improved reconstruction with a large decoder network (10 layers) vs. the small decoder (2 layers). The average pixel error (per channel) of the reconstructed image drops with the larger decoder. In each triplet: (left) original image, (middle) binary image, (right) reconstruction after the decoder. In the last column, a 3x brightened difference-image between the original image and its reconstruction. The improved reconstruction can degrade the faithfulness of the binarized image to the original, since with a larger decoder, the binary image can be more transformed. Top: wood-print *Suruga miho no matsubara* by Ando Hiroshige, 1858. Bottom: watercolor, children’s artwork.

to only two layers from the initial tests with 10 layers). The more transformations the binary image is permitted before reconstruction, the better the reconstruction, but the less the binary image is constrained to represent the original image. See Figure 11. This is an open topic for further research and a new set of applications.

When we allowed the original images to be pre-processed with simple operations (contrast, brightness, saturation, etc), improved results were consistently possible. However, for this paper, we applied *no pre-processing* on the original images to keep the experiments controlled. Methods to automatically pre-process the images before they are given to the neural network is an open, and straightforward, area for future exploration.

Looking towards the aesthetic and artistic potential of this system, consider the image of the blue bench in Figure 9. The strokes appear reminiscent of wood-cuts or the hatching techniques often used in illustrations within historic books and papers (see Appendix). We have not attempted to limit the family of textures permitted in the binarized result, for example, to allow only textures that appear as hatches or cross-hatches. Exploring methods to constrain the set of allowed textures, either programatically or manually, may yield a fruitful avenue for artistic exploration.

## REFERENCES

- [1] Martín Abadi, Paul Barham, Jianmin Chen, Zhifeng Chen, Andy Davis, Jeffrey Dean, Matthieu Devin, Sanjay Ghemawat, Geoffrey Irving, Michael Isard, et al.

2016. Tensorflow: A system for large-scale machine learning. In *12th USENIX Symposium*. 265–283.
- [2] Michael D Abràmoff, Paulo J Magalhães, and Sunanda J Ram. 2004. Image processing with ImageJ. *Biophotonics international* 11, 7 (2004), 36–42.
- [3] Amazon. 2020. Kindle. <https://www.amazon.com/Amazon-Kindle-Ereader-Family/b?ie=UTF8&node=6669702011>. Accessed 10/7/2020.
- [4] Shumeet Baluja. 2019. Hiding images within images. *IEEE transactions on pattern analysis and machine intelligence* 42, 7 (2019), 1685–1697.
- [5] Barnes and Noble. 2020. Nook. [https://www.barnesandnoble.com/b/nook/\\_/N-1pbl](https://www.barnesandnoble.com/b/nook/_/N-1pbl). Accessed 10/7/2020.
- [6] John Bernsen. 1986. Dynamic thresholding of gray-level images. In *Proc. Eighth Int’l conf. Pattern Recognition, Paris, 1986*.
- [7] G. Bradski. 2000. The OpenCV Library. *Dr. Dobb’s Journal of Software Tools* (2000).
- [8] J.H. Campe. 1825. *Life and Adventures of Robinson Crusoe. Latiné scripsit F. J. Goffaux. R. Desilver & T. Desilver*. <https://books.google.com/books?id=AwYKZGuAKq4C>
- [9] Nabendu Chaki, Soharab Hossain Shaikh, and Khalid Saeed. 2014. A comprehensive survey on image binarization techniques. In *Exploring Image Binarization Techniques*. Springer, 5–15.
- [10] C-I Chang, Yingzi Du, J Wang, S-M Guo, and PD Thouin. 2006. Survey and comparative analysis of entropy and relative entropy thresholding techniques. *IEE Proceedings-Vision, Image and Signal Processing* 153, 6 (2006), 837–850.
- [11] Liang-Chieh Chen, George Papandreou, Florian Schroff, and Hartwig Adam. 2017. Rethinking atrous convolution for semantic image segmentation. *arXiv preprint arXiv:1706.05587* (2017).
- [12] Cricut. 2020. Cricut. <https://cricut.com/>. Accessed 10/7/2020.
- [13] Jia Deng, Wei Dong, Richard Socher, Li-Jia Li, Kai Li, and Li Fei-Fei. 2009. Imagenet: A large-scale hierarchical image database. In *Computer Vision and Pattern Recognition, 2009. CVPR 2009. IEEE Conference on*. IEEE, 248–255.
- [14] Oliver Deussen, Marc Spicker, and Qian Zheng. 2017. Weighted linde-buzo-gray stippling. *ACM Transactions on Graphics (TOG)* 36, 6 (2017), 1–12.
- [15] Worthie Doyle. 1962. Operations useful for similarity-invariant pattern recognition. *Journal of the ACM (JACM)* 9, 2 (1962), 259–267.
- [16] eInk.com. 2020. Indoor Large Area Signage. <https://www.eink.com/signage.html?type=application&id=9>. Accessed 10/7/2020.
- [17] Robert Fisher, Simon Perkins, Ashley Walker, and Erik Wolfart. 2017. Image Processing Learning Resources: Adaptive Thresholding. <http://homepages.inf.ed.ac.uk/rbf/HIPR2/adpthrsh.htm>. accessed: 2020-10-5.
- [18] Robert W. Floyd and Louis Steinberg. 1976. An Adaptive Algorithm for Spatial Greyscale. *Proceedings of the Society for Information Display* 17, 2 (1976), 75–77.
- [19] Thomas Funkhouser. 2008. Image Quantization, Halftoning, and Dithering. <https://www.cs.princeton.edu/courses/archive/fall00/cs426/lectures/dither/dither.pdf>, Retrieved on October 5, 2020..
- [20] L. S. G. Kovaszny and H. M. Joseph. 1955. Image Processing. *Proceedings of the IRE* 43, 5 (1955), 560–570. <https://doi.org/10.1109/JRPROC.1955.278100>
- [21] Leon A Gatys, Alexander S Ecker, and Matthias Bethge. 2015. A neural algorithm of artistic style. *arXiv preprint arXiv:1508.06576* (2015).
- [22] Leon A Gatys, Alexander S Ecker, and Matthias Bethge. 2016. Image style transfer using convolutional neural networks. In *Proceedings of the IEEE conference on computer vision and pattern recognition*. 2414–2423.
- [23] Chris A Glasbey. 1993. An analysis of histogram-based thresholding algorithms. *CVGIP: Graphical models and image processing* 55, 6 (1993), 532–537.
- [24] Glowforge. 2020. Glowforge. <https://glowforge.com/>. Accessed 10/7/2020.
- [25] Amy A Gooch, Sven C Olsen, Jack Tumblin, and Bruce Gooch. 2005. Color2gray: salience-preserving color removal. *ACM Transactions on Graphics (TOG)* 24, 3 (2005), 634–639.
- [26] GoodEreader. 2020. GoodEReader. <https://goodereader.com/blog/category/electronic-readers>. Accessed 10/7/2020.
- [27] Ian J Goodfellow, Jean Pouget-Abadie, Mehdi Mirza, Bing Xu, David Warde-Farley, Sherjil Ozair, Aaron Courville, and Yoshua Bengio. 2014. Generative adversarial networks. *arXiv preprint arXiv:1406.2661* (2014).
- [28] Tanner Helland. 2012. Image Dithering: Eleven Algorithms and Source Code. <https://tannerhelland.com/2012/12/28/dithering-eleven-algorithms-source-code.html>. Accessed 10/20/2020.
- [29] Geoffrey Hinton, Nitish Srivastava, and Kevin Swersky. 2012. Neural networks for machine learning. *Coursera, video lectures* 264 (2012).
- [30] Donghui Hu, Liang Wang, Wenjie Jiang, Shuli Zheng, and Bin Li. 2018. A novel image steganography method via deep convolutional generative adversarial networks. *IEEE Access* 6 (2018), 38303–38314.
- [31] Liang-Kai Huang and Mao-Jiun J Wang. 1995. Image thresholding by minimizing the measures of fuzziness. *Pattern recognition* 28, 1 (1995), 41–51.
- [32] Phillip Isola, Jun-Yan Zhu, Tinghui Zhou, and Alexei A Efros. 2017. Image-to-image translation with conditional adversarial networks. In *Proceedings of the IEEE conference on computer vision and pattern recognition*. 1125–1134.
- [33] J Jiang. 1999. Image compression with neural networks—a survey. *Signal Processing: Image Communication* 14, 9 (1999), 737–760.

- [34] Evangelos Kalogerakis, Derek Nowrouzezahrai, Simon Breslav, and Aaron Hertzmann. 2012. Learning hatching for pen-and-ink illustration of surfaces. *ACM Transactions on Graphics (TOG)* 31, 1 (2012), 1–17.
- [35] Jagat Narain Kapur, Prasanna K Sahoo, and Andrew KC Wong. 1985. A new method for gray-level picture thresholding using the entropy of the histogram. *Computer vision, graphics, and image processing* 29, 3 (1985), 273–285.
- [36] Diederik P Kingma and Jimmy Lei Ba. 2015. Adam: A method for stochastic gradient descent. In *ICLR: International Conference on Learning Representations*.
- [37] Josef Kittler and John Illingworth. 1986. Minimum error thresholding. *Pattern recognition* 19, 1 (1986), 41–47.
- [38] Mark Kramer. 1991. Nonlinear principal component analysis using autoassociative neural networks. *AICHE journal* 37, 2 (1991), 233–243.
- [39] Anders Boesen Lindbo Larsen, Søren Kaae Sønderby, and Ole Winther. 2015. Autoencoding beyond pixels using a learned similarity metric. *arXiv preprint arXiv:1512.09300* (2015).
- [40] Sang Uk Lee, Seok Yoon Chung, and Rae Hong Park. 1990. A comparative performance study of several global thresholding techniques for segmentation. *Computer Vision, Graphics, and Image Processing* 52, 2 (1990), 171–190.
- [41] H Li, C and Peter Kwong-Shun Tam. 1998. An iterative algorithm for minimum cross entropy thresholding. *Pattern recognition letters* 19, 8 (1998), 771–776.
- [42] Ming-Yu Liu, Thomas Breuel, and Jan Kautz. 2017. Unsupervised image-to-image translation networks. *arXiv preprint arXiv:1703.00848* (2017).
- [43] F. Lundh, A. Clark, and Contributors. 2019. Pillow (PIL Fork) ImageDraw Module. <https://pillow.readthedocs.io/en/stable/reference/ImageDraw.html>. <https://pillow.readthedocs.io/en/stable/reference/ImageDraw.html>
- [44] Wenjie Luo, Yujia Li, Raquel Urtasun, and Richard Zemel. 2016. Understanding the Effective Receptive Field in Deep Convolutional Neural Networks. In *Advances in Neural Information Processing Systems* 29, D. D. Lee, M. Sugiyama, U. V. Luxburg, I. Guyon, and R. Garnett (Eds.). Curran Associates, Inc., 4898–4906. <http://papers.nips.cc/paper/6203-understanding-the-effective-receptive-field-in-deep-convolutional-neural-networks.pdf>
- [45] Alireza Makhzani, Jonathon Shlens, Navdeep Jaitly, Ian Goodfellow, and Brendan Frey. 2015. Adversarial autoencoders. *arXiv preprint arXiv:1511.05644* (2015).
- [46] David Minnen, George Toderici, Saurabh Singh, Sung Jin Hwang, and Michele Covell. 2018. Image-Dependent Local Entropy Models for Learned Image Compression. *arXiv* (2018). arXiv:1805.12295 [cs.CV]
- [47] W Niblack. 1986. An Introduction to Digital Image Processing (Englewood Cliffs, NJ).
- [48] Onyx. 2020. Boox. <https://www.boox.com/en/>. Accessed 10/7/2020.
- [49] N. Otsu. 1979. A Threshold Selection Method from Gray-Level Histograms. *IEEE Transactions on Systems, Man, and Cybernetics* 9, 1 (1979), 62–66.
- [50] Neerad Phansalkar, Sumit More, Ashish Sabale, and Madhuri Joshi. 2011. Adaptive local thresholding for detection of nuclei in diversity stained cytology images. In *2011 International Conference on Communications and Signal Processing*. IEEE, 218–220.
- [51] Emil Praun, Hugues Hoppe, Matthew Webb, and Adam Finkelstein. 2001. Real-time hatching. In *Proceedings of the 28th annual conference on Computer graphics and interactive techniques*. 581.
- [52] Judith MS Prewitt and Mortimer L Mendelsohn. 1966. The analysis of cell images. *Annals of the New York Academy of Sciences* 128, 3 (1966), 1035–1053.
- [53] Yingge Qu, Wai-Man Pang, Tien-Tsin Wong, and Pheng-Ann Heng. 2008. Richness-preserving manga screening. *ACM Transactions on Graphics (TOG)* 27, 5 (2008), 1–8.
- [54] Wayne S Rasband. 1997. ImageJ. <https://imagej.nih.gov/> U. S. National Institutes of Health, Bethesda, Maryland, USA, Accessed 10/7/2020.
- [55] TW Ridler, S Calvard, et al. 1978. Picture thresholding using an iterative selection method. *IEEE trans syst Man Cybern* 8, 8 (1978), 630–632.
- [56] Nicolas Rougier. 2017. [Re]Weighted voronoi stippling. *The ReScience journal, GitHub* 3, 1 (2017). <https://github.com/ReScience-Archives/Rougier-2017>
- [57] Prasanna K Sahoo, SAKC Soltani, and Andrew KC Wong. 1988. A survey of thresholding techniques. *Computer vision, graphics, and image processing* 41, 2 (1988), 233–260.
- [58] Jaakko Sauvola and Matti Pietikäinen. 2000. Adaptive document image binarization. *Pattern recognition* 33, 2 (2000), 225–236.
- [59] Caroline A Schneider, Wayne S Rasband, and Kevin W Elceiri. 2012. NIH Image to ImageJ: 25 years of image analysis. *Nature methods* 9, 7 (2012), 671–675.
- [60] Adrian Secord. 2002. Weighted voronoi stippling. In *Proceedings of the 2nd international symposium on Non-photorealistic animation and rendering*. 37–43.
- [61] Mehmet Sezgin and Bülent Sankur. 2004. Survey over image thresholding techniques and quantitative performance evaluation. *Journal of Electronic imaging* 13, 1 (2004), 146–166.
- [62] Abhijit G Shanbhag. 1994. Utilization of information measure as a means of image thresholding. *CVGIP: Graphical Models and Image Processing* 56, 5 (1994), 414–419.
- [63] Pierre Soille. 2013. *Morphological image analysis: principles and applications*. Springer Science & Business Media.
- [64] Pavlos Stathis, Ergina Kavallieratou, and Nikos Papamarkos. 2008. An evaluation survey of binarization algorithms on historical documents. In *2008 19th International Conference on Pattern Recognition*. IEEE, 1–4.
- [65] L. Theis, W. Shi, A. Cunningham, and F. Huszár. 2017. Lossy Image Compression with Compressive Autoencoders. In *International Conference on Learning Representations*. <https://openreview.net/pdf?id=rjiNwv9gg>
- [66] George Toderici, Sean M. O’Malley, Sung Jin Hwang, Damien Vincent, David Minnen, Shumeet Baluja, Michele Covell, and Rahul Sukthankar. 2016. Variable Rate Image Compression with Recurrent Neural Networks. *arXiv* (2016). arXiv:1511.06085 [cs.CV]
- [67] Wen-Hsiang Tsai. 1985. Moment-preserving thresholding: A new approach. *Computer Vision, Graphics, and Image Processing* 29, 3 (1985), 377–393.
- [68] F. H. Van. 1695. *Deliciae Musicae: The second book*. 2. 1695. John Heptinstall for Henry Playford. <https://books.google.com/books?id=k8agLwx1DIC>
- [69] Panqu Wang, Pengfei Chen, Ye Yuan, Ding Liu, Zehua Huang, Xiaodi Hou, and Garrison Cottrell. 2018. Understanding convolution for semantic segmentation. In *2018 IEEE winter conference on applications of computer vision (WACV)*. IEEE, 1451–1460.
- [70] Wikipedia. 2020. E Ink. [https://en.wikipedia.org/wiki/E\\_Ink](https://en.wikipedia.org/wiki/E_Ink). Wikipedia: The Free Encyclopedia. Accessed 10/7/2020.
- [71] Wikipedia. 2020. Hatching. <https://en.wikipedia.org/wiki/Hatching> Wikipedia: The Free Encyclopedia. Accessed 10/23/2020.
- [72] Menghan Xia, Xueting Liu, and Tien-Tsin Wong. 2018. Invertible grayscale. *ACM Transactions on Graphics (TOG)* 37, 6 (2018), 1–10.
- [73] Jui-Cheng Yen, Fu-Juay Chang, and Shyang Chang. 1995. A new criterion for automatic multilevel thresholding. *IEEE Transactions on Image Processing* 4, 3 (1995), 370–378.
- [74] Gregory W Zack, William E Rogers, and Samuel A Latt. 1977. Automatic measurement of sister chromatid exchange frequency. *Journal of Histochemistry & Cytochemistry* 25, 7 (1977), 741–753.
- [75] Johannes Zander, Tobias Isenberg, Stefan Schlechtweg, and Thomas Strothotte. 2004. High quality hatching. *Computer Graphics Forum* 23, 3 (2004), 421–430.
- [76] Jun-Yan Zhu, Taesung Park, Phillip Isola, and Alexei A Efros. 2017. Unpaired image-to-image translation using cycle-consistent adversarial networks. In *Proceedings of the IEEE international conference on computer vision*. 2223–2232.



## A APPENDIX

The next 9 pages illustrate the binarization of artworks and photographs. They are shown expanded so that the textures created can be examined. Please note how different colors are handled. The sharp boundaries in the original image are recreated through the use of distinct textures. Gradual fades are represented by textures that change slowly, thereby allowing for seamless overlap.

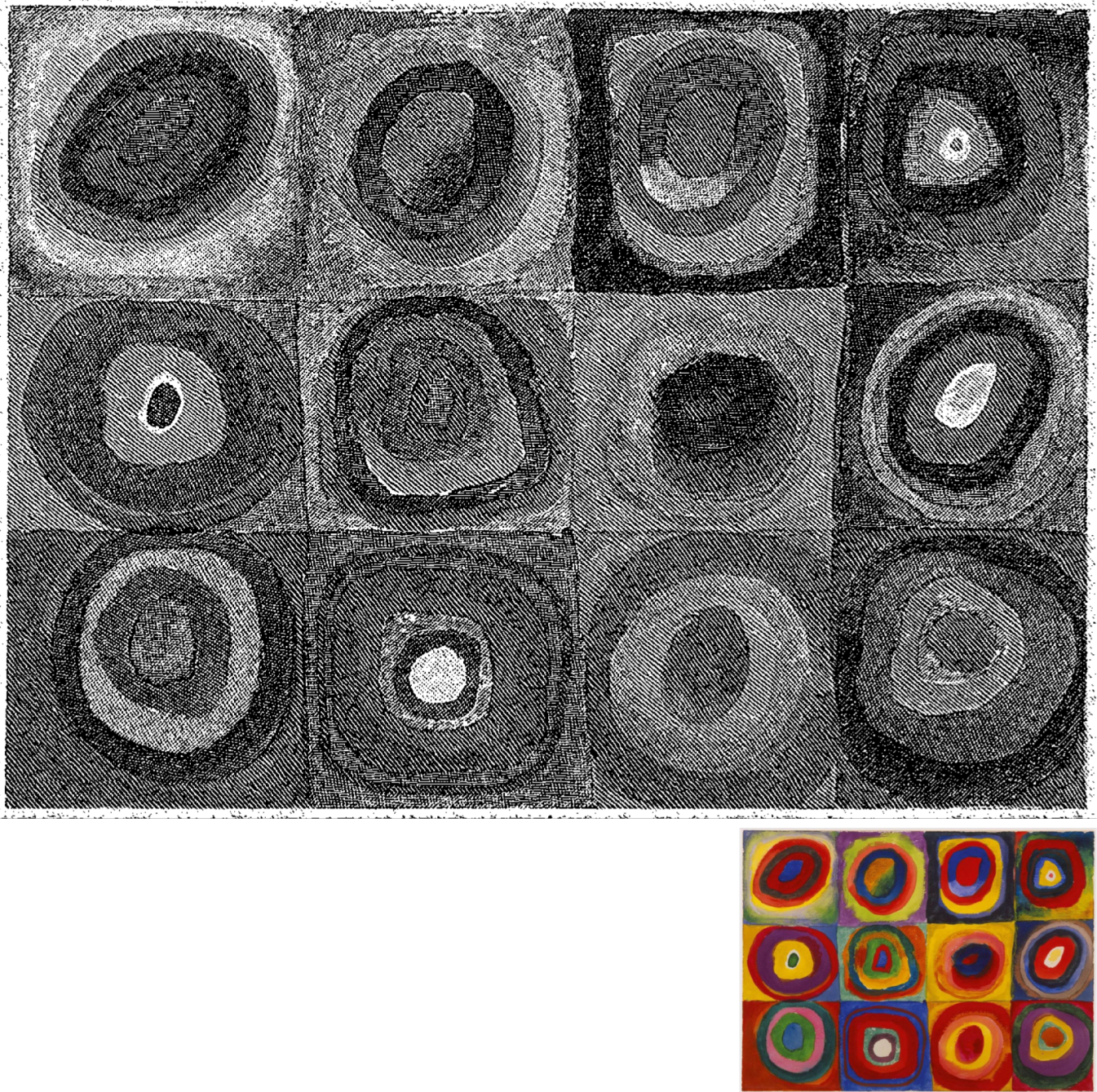


**Figure 12:** *Color Study. Squares with Concentric Circles* (1913) Wassily Kandinsky.



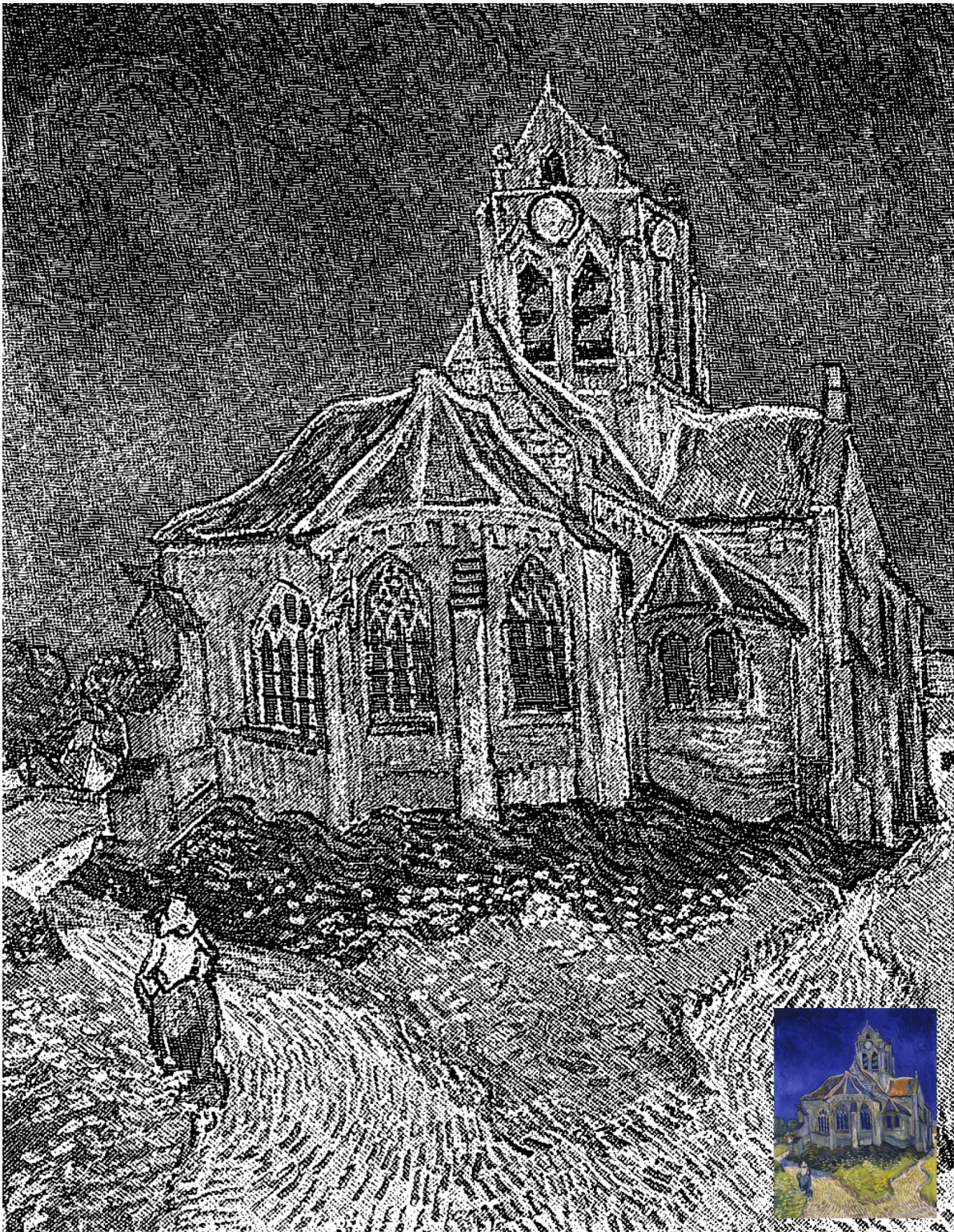


**Figure 13:** *The Church at Auvers* (1890) by Vincent van Gogh



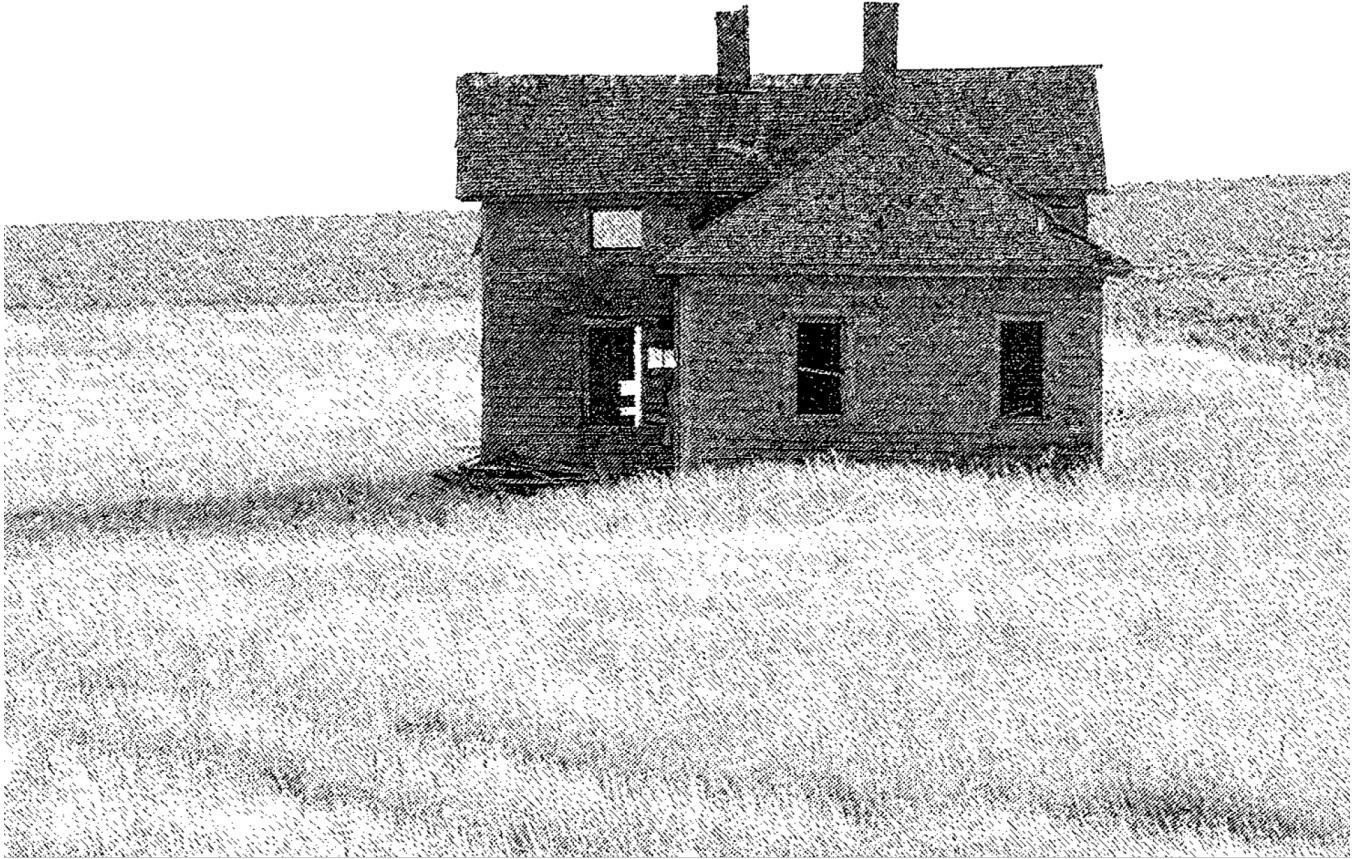


**Figure 14:** Photograph of a burned house (2003)





**Figure 15:** *The Old Guitarist* (1903) Pablo Picasso



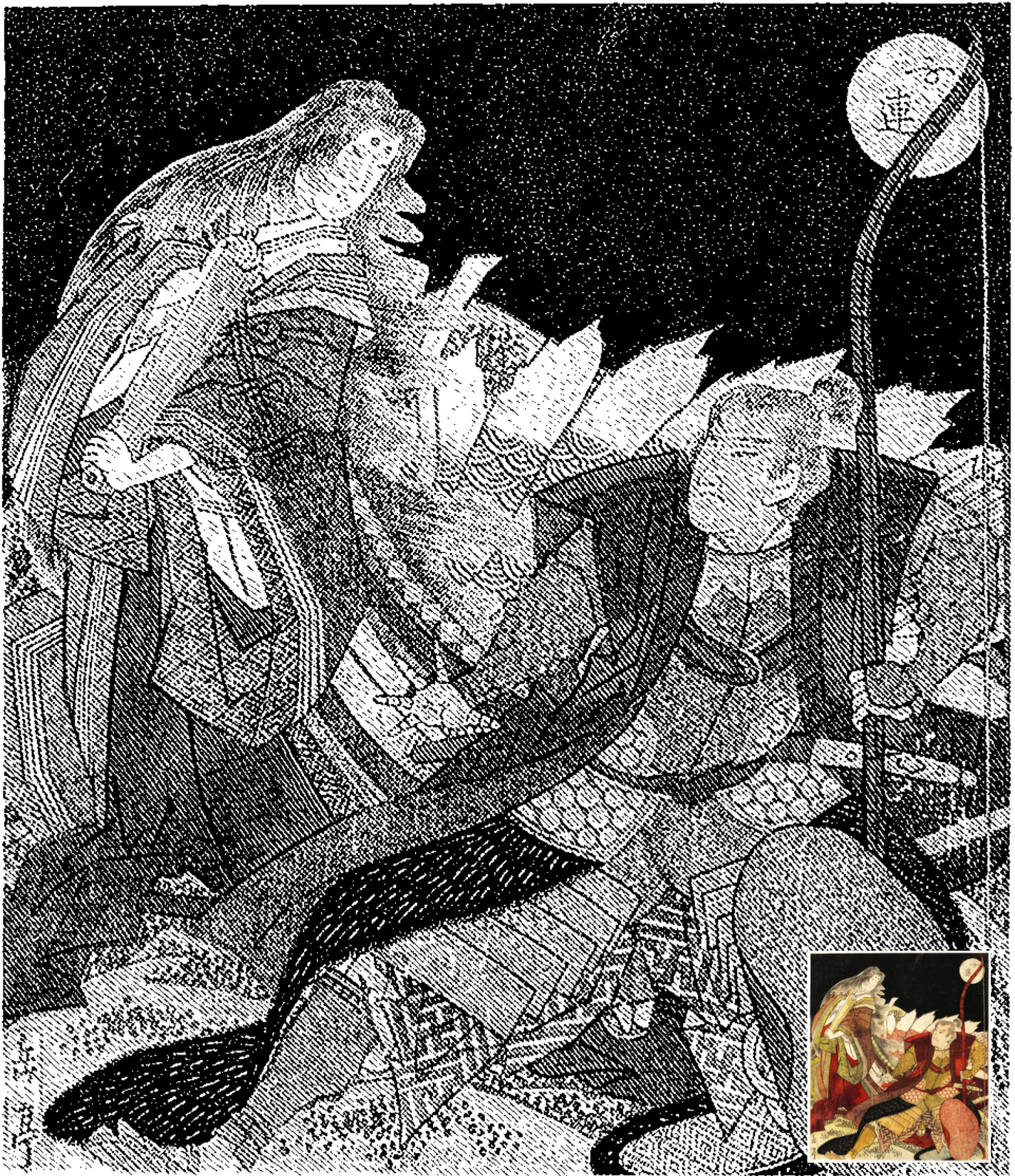


**Figure 16:** *The Warrior Miura-no-suke Confronting the Court Lady Tamamo-no-ma* (1820) by Yashima Gakutei



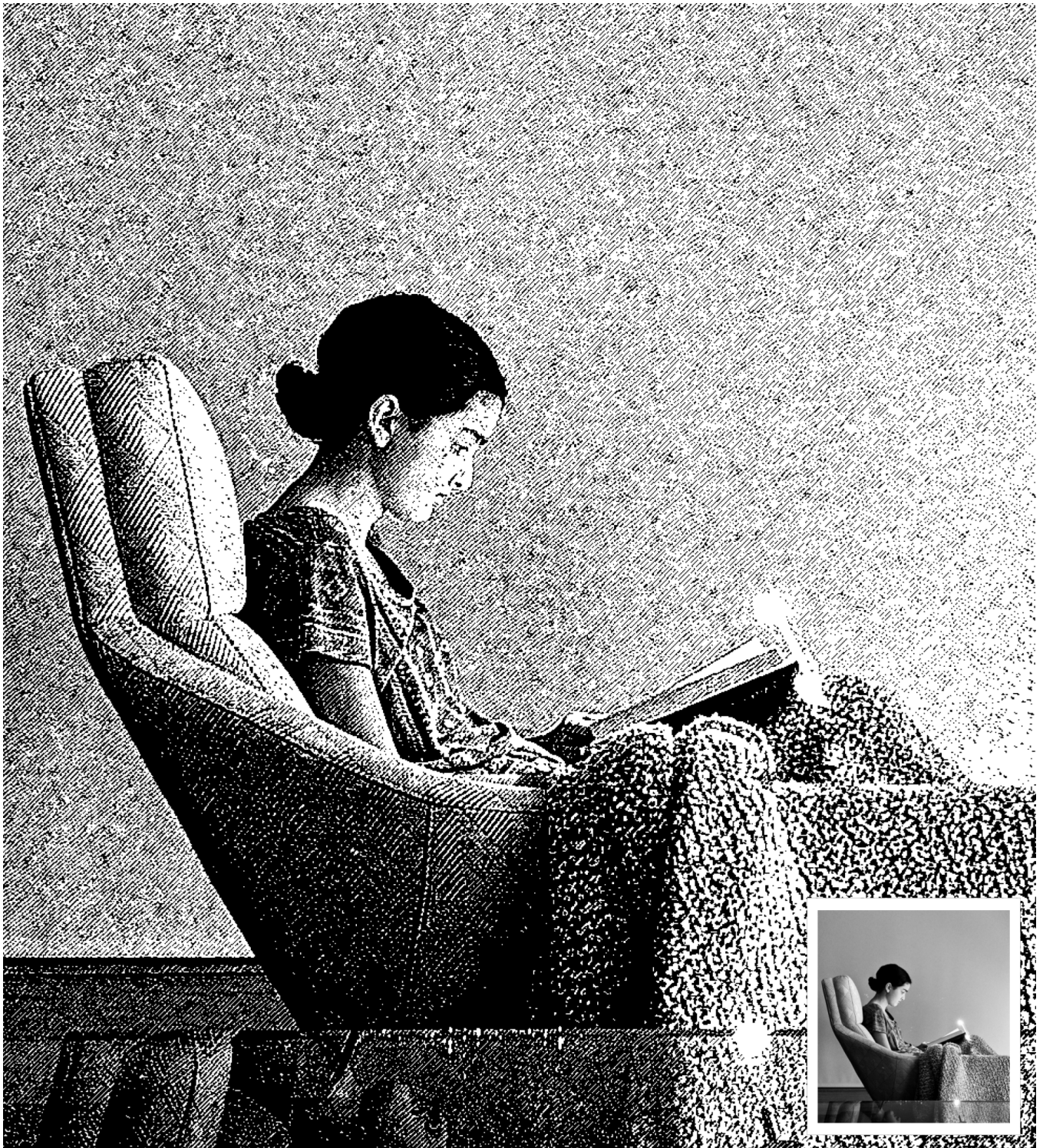


**Figure 17:** Black and white photograph of a young girl reading (2020)



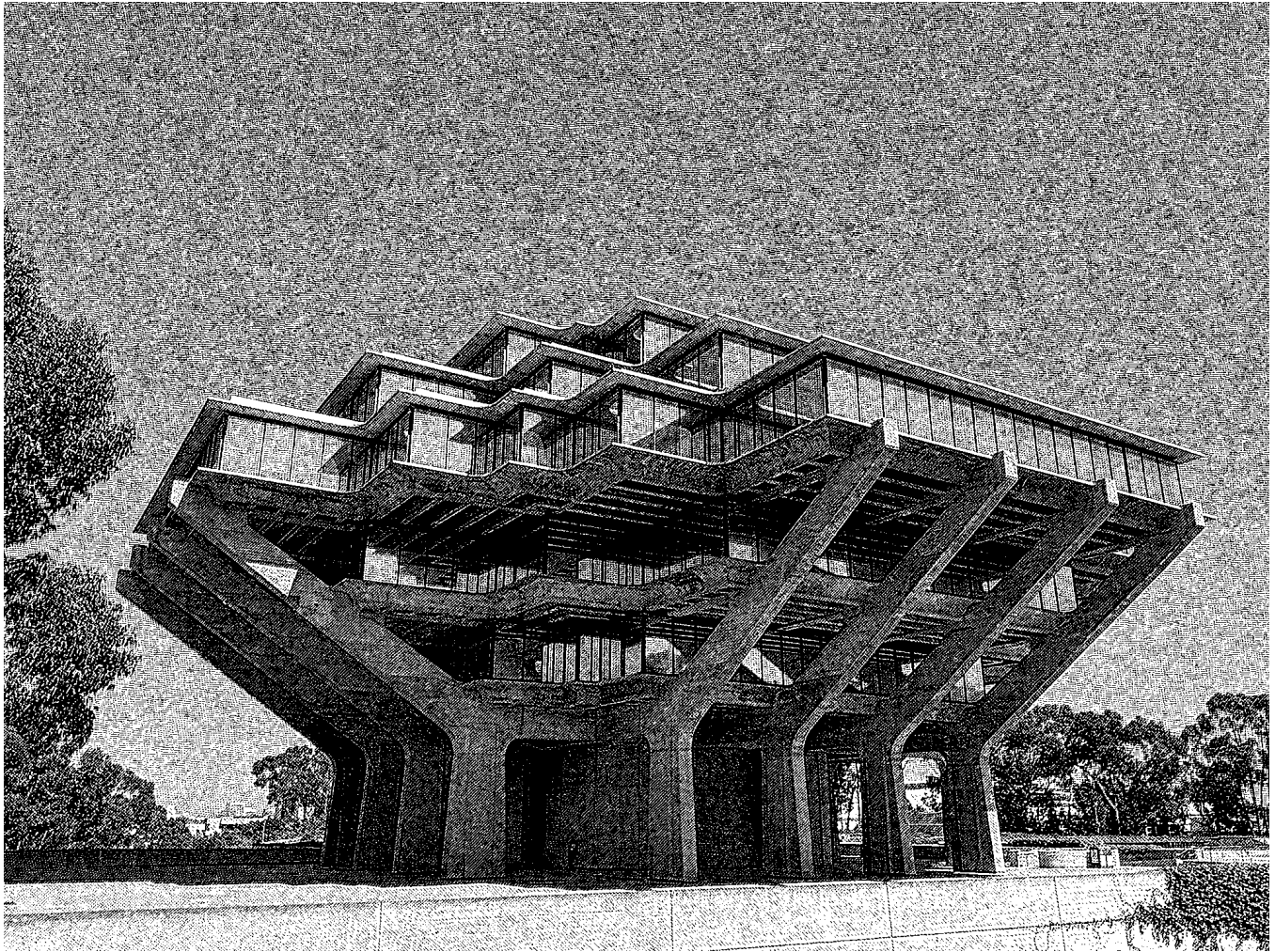


**Figure 18:** Color photograph (2021).





**Figure 19:** Color photograph (2021).



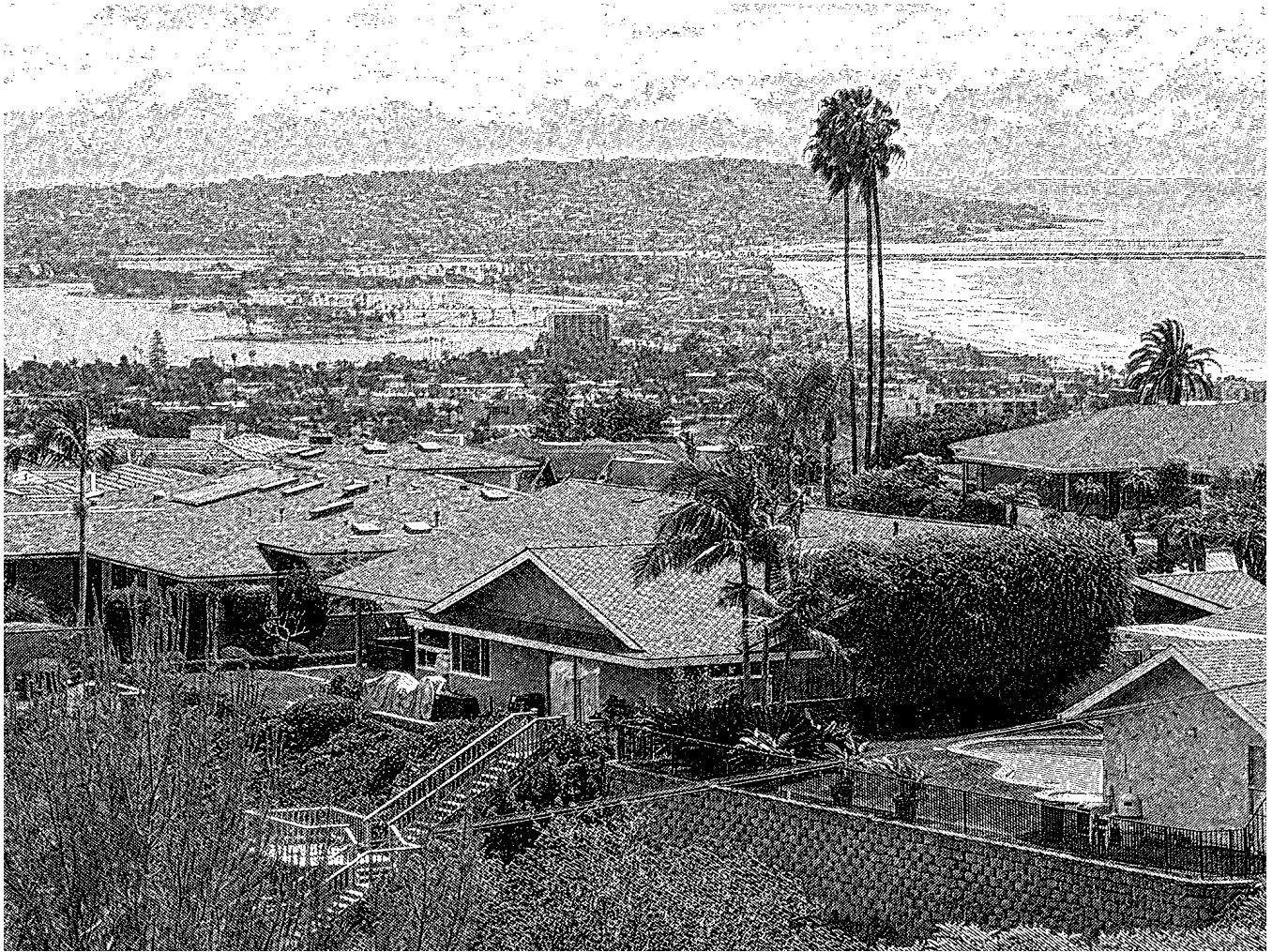


**Figure 20:** Color photograph (2021).

## A.1 Historic uses of Hatching and Cross-Hatching



**Figure 21:** Three historic uses of hatching and cross-hatching. (a) From 1695 book *Deliciae Musicae: The second book* [68] (b) from Campe, J.H. (1825) [8] (c) *A Man with a Short Beard and Embroidered Cloak* (1631) by Rembrandt.